This is a repository copy of *Recent Development of Reluctance Machines with Different Winding Configurations, Excitation Methods, and Machine Structures*.

Article:

Recent Development of Reluctance Machines with Different Winding Configurations, Excitation Methods, and Machine Structures

X. Y. Ma, G. J. Li, Senior Member, IEEE, G. W. Jewell, and Z. Q. Zhu, Fellow, IEEE

Department of Electronic & Electrical Engineering, The University of Sheffield, Sheffield, UK

g.li@sheffield.ac.uk

Abstract—**This paper reviews the performances of some newly developed reluctance machines with different winding configurations, excitation methods, stator and rotor structures, and slot/pole number combinations. Both the double layer conventional (DLC-), double layer mutually-coupled (DLMC), single layer conventional (SLC-), and single layer mutually-coupled (SLMC-), as well as fully-pitched (FP) winding configurations have been considered for both rectangular wave and sinewave excitations. Different conduction angles such as unipolar 120° elec., unipolar/bipolar 180° elec., bipolar 240° elec. and bipolar 360° elec. have been adopted and the most appropriate conduction angles have been obtained for the SRMs with different winding configurations. In addition, with appropriate conduction angles, the 12-slot/14-pole SRMs with modular stator structure is found to produce similar average torque, but lower torque ripple and iron loss when compared to non-modular 12-slot/8-pole SRMs. With sinewave excitation, the doubly salient synchronous reluctance machines with the DLMC winding can produce the highest average torque at high currents and achieve the highest peak efficiency as well. In order to compare with the conventional synchronous reluctance machines (SynRMs) having flux barriers inside the rotor, the appropriate rotor topologies to obtain the maximum average torque have been investigated for different winding configurations and slot/pole number combinations. Furthermore, some prototypes have been built with different winding configurations, stator structures, and slot/pole combinations to validate the predictions.**

Keywords—**Double/single layer windings, excitation methods, fully/short-pitched, mutually coupled, modular machines, switched/synchronous reluctance machines.**

Nomenclature

SRM	Switched Reluctance Machine
DSRM	Doubly-salient Synchronous Reluctance Machine
SynRM	Synchronous Reluctance Machine
DLC	Double Layer Conventional
DLMC	Double Layer Mutually Coupled
SLC	Single Layer Conventional
SLMC	Single Layer Mutually Coupled
FP	Fully-Pitched
AFB	Angled flux barrier
RFB	Round flux barrier
FG	Flux gap

I. INTRODUCTION

With no permanent magnets or field windings on the rotors, the switched reluctance machines (SRMs) have very simple and robust structures [1] - [2]. As a result, they can be used in a variety of applications such as the automotive, renewable energy, aerospace and domestic appliances sectors [3] - [4]. However, with doubly salient structure, the SRMs can have abrupt change in radial force acting on the stator. In addition, the unipolar phase current waveforms of the SRMs (usually 120 degrees conduction for 3-phase SRMs) can have the abrupt change in phase current as well. As a result, the SRMs tend to exhibit higher levels of vibrations and acoustic noise when compared to permanent magnet machines and induction machines [5] [6] [7] [8]. Moreover, the nonconventional power-converter used for conventional SRMs drive system is to some extent limit its foothold in the market. Similar to the SRMs, the synchronous reluctance machines (SynRMs) have magnet-free features but are supplied with sinewave currents. Hence, the off-the-shelf 3-phase standard inverters like that used in other synchronous machines can be used to drive the SynRMs [6] [9] [10]. Different from the SRMs, most SynRMs have flux barriers inside the rotors such as round flux barrier (RFB) or angled flux barrier (AFB) inside the rotor iron core [9] [11] [12]. However, the complicated rotor structure could not be manufactured as easy as that of SRMs, leading to lower manufacturability and potentially higher manufacturing cost. In order to employ a standard 3-phase inverter for reducing the system cost and the doubly-salient machine structure for simpler manufacturing, the SRMs have been supplied with sinewave currents in [10] and [13] which are in effect doubly-salient synchronous reluctance machines (DSRMs) but with short-pitched and concentrated windings.

Similar to the induction machines, the distributed stator windings are often employed in conventional SynRMs [14]. However, the fractional-slot concentrated windings are adopted to many permanent magnet machines and SRMs due to their inherent advantages such as higher slot packing factor, shorter end-winding, smaller machine overall size, etc. [15] [16] [17]. For the DSRMs, both the short-pitched concentrated windings and the fully-pitched distributed windings can be employed and this has been investigated in literature [18] [19] [20]. It has been found that the DSRM equipped with short-pitched, double layer mutually coupled (DLMC) winding is less sensitive to magnetic saturation than the ones with the double layer conventional (DLC) windings and hence, can have better overload capability [2] [13]. Nevertheless, the torque ripple of the DSRM equipped with

the DLMC windings is relatively higher due to its nature of self- and mutual-inductances. While with fully-pitched (FP) winding, the DSRM can generate lower torque ripple but its long end-winding will lead to higher copper loss for a given phase current. In order to take advantage of both the DL concentrated windings (shorter end-winding) and the FP distributed windings (higher torque capability), the DSRM with single layer conventional (SLC) and single layer mutually-coupled (SLMC) windings have been proposed in [20].

In this paper, all of these winding configurations (DLC, DLMC, FP, SLC and SLMC) will be employed for both the SRMs (with rectangular wave excitation) and DSRM (with sinewave excitation). For SRMs, the appropriate conduction angles will be obtained and the electromagnetic performance will be compared to modular SRMs with different slot/pole number combinations. For the DSRMs, their electromagnetic performance will be compared between different winding configurations. In addition, when compared to the SynRMs with RFB (SynRM-RFB) and AFB (SynRM-AFB), the appropriate rotor structures will be obtained for different winding configurations and slot/pole number combinations.

II. WINDING CONFIGURATIONS AND THEIR INFLUENCE ON INDUCTANCES AND PHASE RESISTANCES

A. Winding Configurations

As mentioned previously, both the DLC/SLC windings, and the DLMC/SLMC windings, as well as the FP winding have been employed with both rectangular wave and sinewave excitations for more comprehensive investigation in this paper. For consistency and clarity, all the machines have the same leading dimensions and design features as listed in TABLE I. The dimensions such as split ratio, stator/rotor tooth width, and stator/rotor back iron, shaft outer radius, etc., have been optimized separately for different machine structures.

TABLE I MACHINE LEADING DIMENSIONS AND DESIGN FEATURES

Stator slot number	12	Active length (mm)	60
Rotor pole number	4/8/10/14/16	Turn number per phase	132
Stator outer radius (mm)	45	Coil packing factor	0.37
Air gap length (mm)	0.5	Rated RMS current (A)	10

In order to observe the influence of winding configurations on the flux distributions, the 3-phase 12-slot/8-pole SRMs have been selected for illustration. As can be seen from Fig. 1, the rotors are at aligned position and the phase A is supplied with a 10A dc current. Fig. 1 (a) and (b) are the DLC-SRM and DLMC-SRM, in which each stator tooth is wound with one coil and each phase has four concentrated coils connected in series. Thus, two coils of two different phases are located in each stator slot, leading to a DL winding. In addition, the coil pitch is smaller than the pole pitch, leading to a short-pitched winding. In contrast, for the FP-SRM in Fig. 1 (e), each phase winding consists of two coils and each coil spans three slot pitches, leading to a FP winding. In addition, it can be regarded as a SL winding since

only one coil is located in each stator slot. However, with distributed winding, the significant longer end-windings of the FPSRM can result in higher copper loss than the DL-SRMs at the same phase current. In order to avoid long end-windings, the SLC-SRM and SLMC-SRM as shown in Fig. 1 (c) and (d) have been proposed with short-pitched windings which are derived from the DLC-SRM and DLMC-SRM but with SL winding structure. As a result, each phase of the SL-SRMs has two coils and each coil is wound around one stator tooth, leading to concentrated winding structure. Similar to the FP-SRM, the SL-SRMs have only one coil located in one stator slot, hence, the number of the turns per coil is twice as that of the DL-SRMs. Moreover, with single layer structure, both the FP-SRM and SL-SRMs have the potential to produce higher average torque than that of the DL-SRMs without magnetic saturation, as will detailed in this paper. In contrast, the less MMF concentration in the DL-SRMs indicates less flux density, and hence less sensitivity to magnetic saturation, in particular the DLMC-SRM can have better overload torque capability.
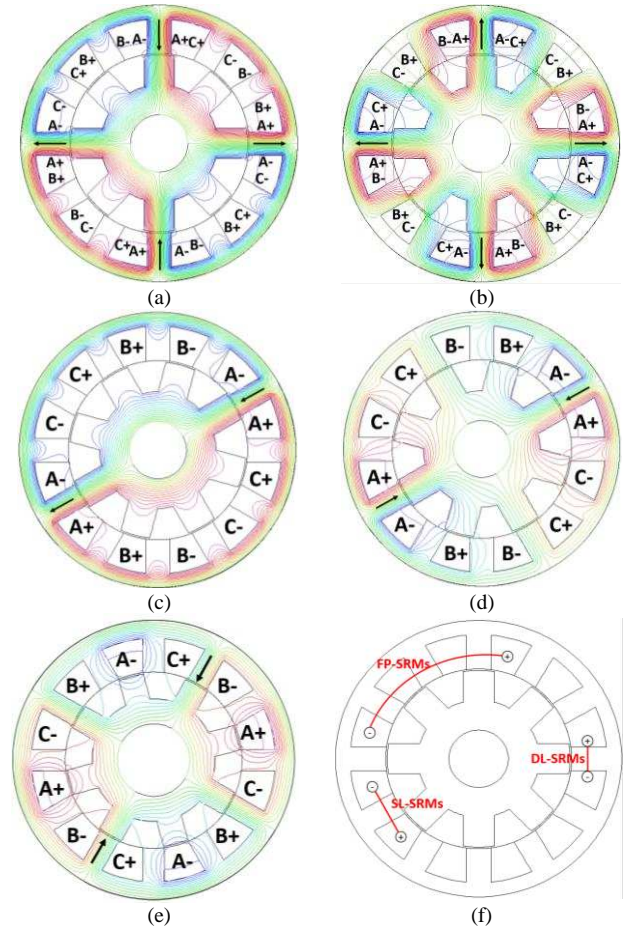

Fig. 1. Flux distributions of 3-phase 12-slot/8-pole SRMs with different winding configurations. (a) DLC-SRM, (b) DLMC-SRM, (c) SLC-SRM, (d) SLMC-SRM and (e) FP-SRM. The rotor is at aligned position and only the phase A is supplied with a 10A dc current. (f) examples of end-winding of different SRMs.

The difference between the DLC/SLC and the DLMC/SLMC windings results in different flux paths (as shown in Fig. 1) and also different coil magnetic polarities (as shown in TABLE II). With conventional windings, there is almost no mutual-flux between phases, as shown in Fig. 1

(a) and (c). However, with mutually-coupled windings and also the FP winding, the flux of phase A also links to phases B and C. As a result, mutual flux exists and this could potentially contribute to higher on-load torque if appropriate excitation is selected.

TABLE II INFLUENC OF WINDING CONFIGURATIONS ON COIL MAGNETIC POLARITIES OF THE PHASE A

Winding configurations	Coil magnetic polarities
DLC	SNSN
DLMC	SSSS
SLC	NS
SLMC	NN
FP	NS

B. Influence of Winding Configurations on Inductances and Phase Resistances

1) Derivatives of Self- and Mutual- Inductances

Different winding configurations result in different flux paths, and hence influence the self-inductance L and mutual-inductance M, which have been calculated using 2-D finite element analysis (FEA) as shown in Fig. 2(a) and Fig. 3(a). The derivatives of self- and mutual-inductances with respect to rotor positions ($dL/d\theta$ and $dM/d\theta$), which directly contribute to the electromagnetic torque as can be seen from (1), have been calculated as shown in Fig. 3(b) and Fig. 3(b), where the rotor position of 0 elec. deg. represents the rotor aligned position.

$$T = \overbrace{\frac{1}{2}i_a^2\frac{dL_a}{d\theta} + \frac{1}{2}i_b^2\frac{dL_b}{d\theta} + \frac{1}{2}i_c^2\frac{dL_c}{d\theta}}^{T_{self}} \quad (1)$$
$$\underbrace{+ i_a i_b \frac{dM_{ab}}{d\theta} + i_b i_c \frac{dM_{bc}}{d\theta} + i_a i_c \frac{dM_{ac}}{d\theta}}_{T_{mutual}}$$

As can be found in Fig. 3(b) that the amplitudes of $dL_a/d\theta$ of the SLC-SRM and the SLMC-SRM are higher than those of their DL counterparts, respectively. Therefore, it can be predicted that the SRMs with SL winding structures could produce higher torque by self-inductance (self-torque) than their DL counterparts. Moreover, with higher amplitude of $dL_a/d\theta$, the self-torque of the CSRMs could be predicted to be slightly higher than that of the MCSRMs, regardless of DL or SL winding structure. However, it can be seen from Fig. 3(b) that $dM_{ab}/d\theta$ of the CSRMs are almost null, while it is apparent in the MCSRMs due to its nature of mutual flux. As a result, the torque produced by mutual-inductance (mutual-torque) of the MCSRMs have the potential to contribute to the resultant torque since the $dM_{ab}/d\theta$ is proportional to the mutual-torque without magnetic saturation. However, the mutual-torque in the CSRMs is close to zero. Therefore, the MCSRMs have the potential to produce higher resultant torque than the CSRMs since both $dL_a/d\theta$ and $dM_{ab}/d\theta$ could contribute to the torque. For the FP-SRMs, $dL_a/d\theta$ has different frequency from other machines so that it is negligible for torque production. However, its significantly higher amplitude of $dM_{ab}/d\theta$ would still allow it to achieve better torque performance.
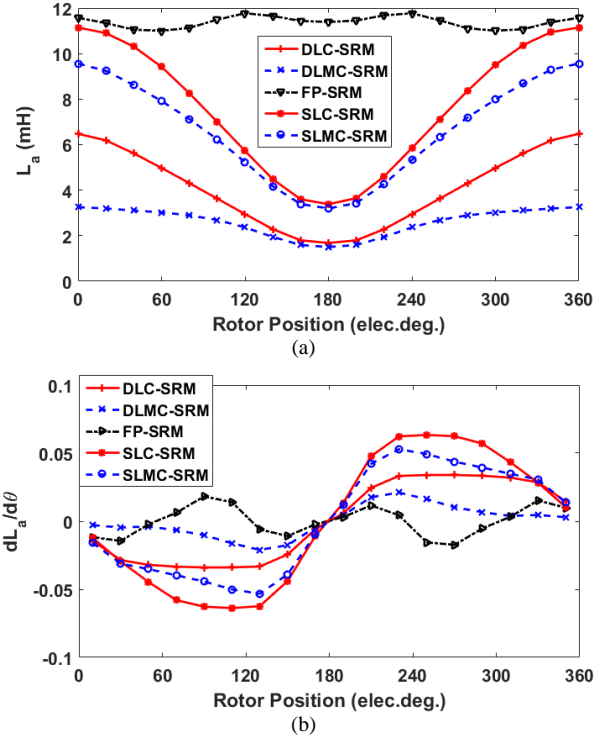

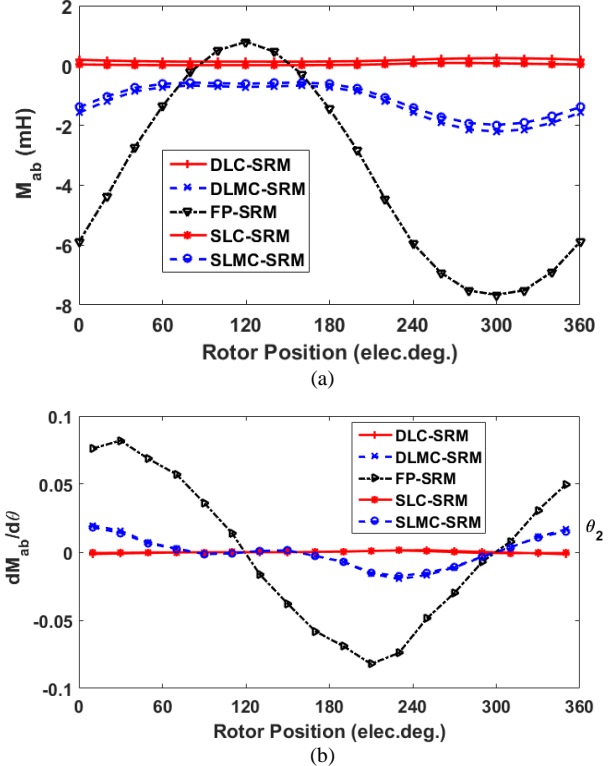Fig. 2. Comparison of (a) L_a and (b) $dL_a/d\theta$. Phase A is supplied with a 10A dc current.

Fig. 3. Comparison of (a) M_{ab} and (b) $dM_{ab}/d\theta$. Phase A is supplied with a 10A dc current.

2) Phase Resistances

Phase resistance depends on the mean length per turn, which consists of two active conductors in stator slots and two end-windings. Fig. 1(f) shows examples of end-windings of different winding configurations. For a given sized

machine, the end-winding is influenced by the winding configurations and largely determines the copper loss.

Accordingly, TABLE III summarizes the average value of one end-winding length of both the DL and SL, as well as the FP-SRMs, where W_s is average stator slot width (trapezoidal slot shape) and W_t is stator tooth width. For the FPSRM, the end winding consists of $\frac{1}{2}\pi W_s$ plus an arc length of the span range of a coil where S_i is the stator inner radius, h_s is the slot height, N_s is the slot number, and γ is the slot opening in mechanical degree. It can be found that the end-windings of the SL-SRMs are slightly higher than that of the DL-SRMs, but are significantly shorter than that of the FP-SRM. In addition, the FP-SRM has the longest mean length per turn which consists of two end winding length plus two active length. As a result, the FP-SRM has the highest phase resistance. In addition, the DL winding has the lowest phase resistance amongst all the winding configurations, and hence could produce the lowest copper loss at the same phase current.

TABLE III INFLUENCE OF WINDING CONFIGURATIONS ON END-WINDINGS AND PHASE RESISTANCE WITH COIL TEMPERATURE @ 20℃

Winding configurations	End-windings	Mean length per turn (m)	Phase Resistance (Ω)
DL	$\frac{1}{4}\pi W_s + W_t$	0.15	0.53
SL	$\frac{1}{2}\pi W_s + W_t$	0.17	0.57
FP	$\frac{1}{2}\pi W_s + 2\pi(S_i + \frac{1}{2}h_s)$ $\times \frac{360°/N_s \times 3 - \gamma}{360°}$	0.24	0.82

III. SRMs WITH RECTANGULAR WAVE EXCITATION

A. Conduction Angles

With different winding configurations, the SRM can be supplied with rectangular wave excitation with various conduction angles. It is well-established that the unipolar 120° elec. conduction is usually adopted for the 3-phase CSRMs, in which only the contribution of the self-inductances to the electromagnetic torque is considered. However, as mentioned previously, the electromagnetic torque can be determined by both the derivatives of self- and mutual-inductances. Thus, conduction angles such as unipolar 180° elec., bipolar 180° elec., bipolar 240° elec. and bipolar 360°, as shown in Fig. 4, have been selected for the SRMs with different winding configurations in order to achieve higher resultant torque (self-torque + mutual-torque).

B. Influence of Winding Configurations on SRMs' Performance

According to the current waveforms shown in Fig. 4, the electromagnetic torque can be calculated by 2-D FEA for the SRMs with different windings. TABLE IV summarizes the machine average torques with different conduction angles.

It can be found that the FP-SRM with bipolar 360° elec. conduction can have the best torque performance, while the unipolar 120° elec. is the worst due to negligible contribution of self-inductance in FP-SRM. In contrast, with nearly null mutual-inductance, the unipolar 120° elec. conduction is the most appropriate one for the DLC-SRM. While for the DLMC-SRM, the bipolar 240° elec. conduction is the most appropriate one, in which the contributions of both the self- and mutual-inductances have been considered. Similar to the DLC-SRM, the SLC-SRM produces the highest average torque with the unipolar 120° elec. conduction at low current levels ($10A_{rms}$), while the unipolar 180° elec. becomes the most appropriate conduction angles at high current levels ($40A_{rms}$), due to magnetic saturation. Moreover, the SLMC-SRM with bipolar 180° conduction achieves its best performance at both low and high current levels.
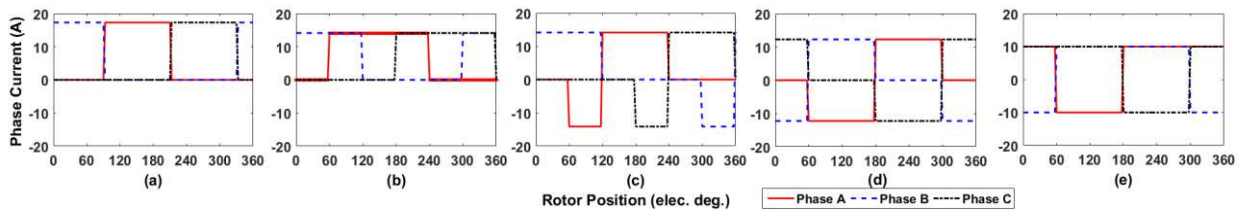

Fig. 4. Rectangular wave excitation with different conduction angles. (a) Unipolar 120°elec., (b) unipolar 180°elec., (c) bipolar 180°elec., (d) bipolar 240°elec., and (e) bipolar 360°elec.

TABLE IV   SUMMARY OF MACHINE AVERAGE TORQUE WITH DIFFERENT CONDUCTION ANGLES

	DLC-SRM		DLMC-SRM		FP-SRM		SLC-SRM		SLMC-SRM	
	Low current	High current	Low current	High current	Low current	High current	Low current	High current	Low current	High current
Unipolar 120°	1	1	4	4	5	5	1	2	2	2
Unipolar 180°	2	2	5	5	2	2	2	1	4	4
Bipolar 180°	3	3	2	2	4	4	3	3	1	1
Bipolar 240°	4	4	1	1	3	3	4	4	3	3
Bipolar 360°	5	5	3	3	1	1	5	5	5	5

Note: Number 1-5 represents relative average torque from the highest to the lowest.

C. Novel Modular SRMs for Performance Improvement

In order to maintain or even enhance the machine performance while achieving high fault tolerant capability, novel modular, single layer winding SRMs with different pole numbers are proposed, which are also supplied by rectangular wave current with different conduction angles. By way of example, the 3-phase 12-slot/14-pole SRM with non-modular and E-core modular machine structures are shown in Fig. 5 (a) and (b), respectively.

In order to maintain the similar level of magnetic saturation in stator teeth with flux gaps (FGs), the stator tooth body iron section width W_t will be kept constant for different FG widths. In addition, it is worth mentioning that for a fixed Ampere-Turn per slot, the current density will be increased with the increasing FG width due to the reduced slot area (increased from $5.68A_{rms}/mm^2$ to $7.33A_{rms}/mm^2$ with increasing FGs from 0mm to 6mm).
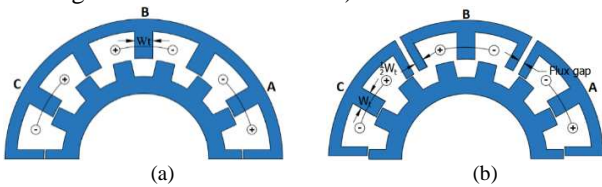

Fig. 5. Cross-sections (half) of the 12-slot/14-pole SRMs with (a) non-modular structures, (b) modular structures. All the machines have the SLC winding topologies.

For clarity, a diagram including FGs, slot/pole number combinations, winding configurations, and conduction angles for all the investigated modular SRMs is shown in Fig. 6. The trends of electromagnetic performance of 12-slot/10-pole and 12-slot/16-pole machines with different FGs are not shown in this paper, since they are very similar to those of the 12-slot/8-pole and 12-slot/14-pole machines, respectively. For consistency and fair comparison between non-modular (FG=0mm) and modular (FG>0mm) machines, the most appropriate conduction angle for high current has been employed. According to TABLE IV, the unipolar 180° elec. and bipolar 180° elec. conductions have been selected for the 12-slot/8-pole conventional and mutually-coupled winding machines, respectively. However, for the 12-slot/14-pole machines, the bipolar 180° elec. conduction is adopted for the CSRMs, while the unipolar 180° elec. conduction is for the MCSRMs.
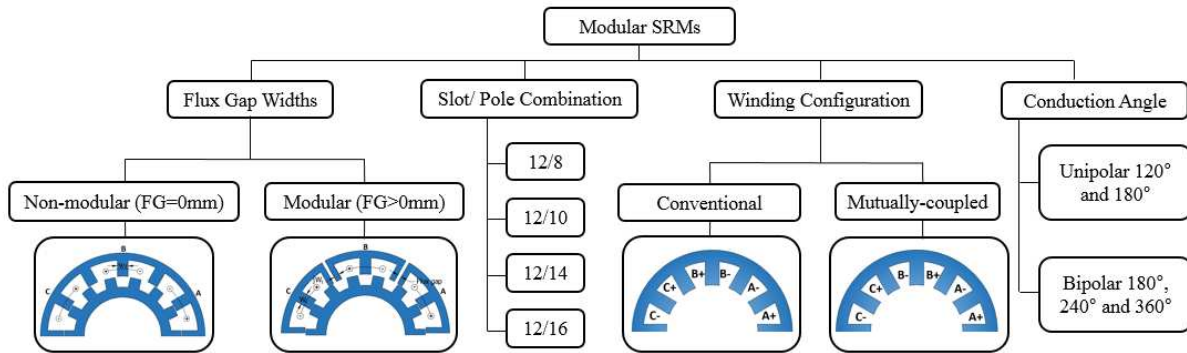

Fig. 6. Investigation variables of the modular SRMs. The SRMs are equipped with rectangular excitation.

1) Average Torque and Torque Ripple Against Copper Loss

With the appropriate conduction angle, the average torque and torque ripple can be obtained by 2-D FEA at different current levels. It is found that the 12-slot/8-pole SRM with non-modular structure achieves better performance than its modular counterpart regardless of the employed phase RMS current and the winding configuration. However, for a full range of currents, the 12-slot/14-pole conventional SRM with FG=3 mm has the best torque performances considering both the average torque and torque ripple while for the MCSRM, it is FG=5mm. Hence, the modular machine with FG=3 mm and FG=5 mm have been selected for both the CSRMs and MCSRMs respectively, for overload torque capacity and copper loss calculation.

It is evident that the copper losses for all modular machines are higher than those of their non-modular counterparts at the same current, regardless of the pole numbers. This is due to the fact that with increasing FG width, the slot area is slightly reduced, leading to reduced wire diameter. However, the average torque is also influenced by the FGs. Hence, in order to provide a consistent basis for comparison, the relationship between torque and copper loss has been investigated.

With the appropriate conduction angles and FG widths, the variation in the average torques as a function of copper loss for a non-modular 8-pole SRM and a modular 14-pole SRM with both conventional and mutually-coupled windings are shown in Fig. 7. It is apparent that both non-modular and modular machines can produce similar average torque values for the same copper loss, regardless of winding configurations. However, with conventional winding, the torque ripple in modular 12-slot/14-pole machine can be much lower than that in non-modular 12-slot/8-pole machine when the copper loss (phase current) is higher than around 170W (10A). While, the torque ripple in modular 12-slot/14-pole machine can be much lower than that in non-modular

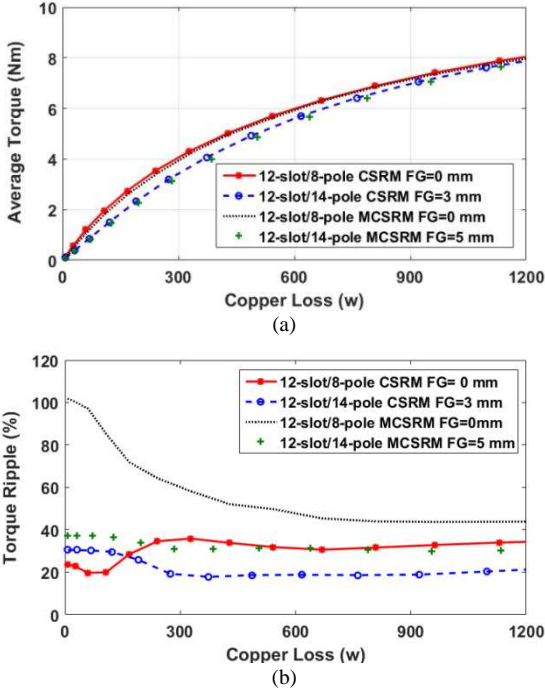12-slot/8-pole machine at any copper loss (phase current) with mutually-coupled winding configurations.

(a)

(b)

Fig. 7. Comparison of (a) average torque and (b) torque ripple (calculated by $\frac{T_{max}-T_{min}}{T_{av}} \times 100\%$ where T_{max}, T_{min} and T_{av} are the maximum, minimum and average torque over an electrical period) as a function of SRM copper loss.

2) Iron Loss

In addition, iron loss has been calculated for the investigated modular and non-modular machines. Fig. 8 and Fig. 9 show the iron loss against phase RMS current and speed for conventional modular SRMs with different FGs. Due to similar trend in iron loss, the results for MCSRMs are not shown in this paper to avoid duplication. It can be found that the 12-slot/14-pole machine produces higher iron loss than the 12-slot/8-pole machine due to the higher stator flux density frequency. However, both machines produce significantly lower iron losses with increasing FGs. For example, the iron loss of the modular 12-slot/14-pole CSRM with FG=2mm is reduced by around 63% when compared to the non-modular CSRM with FG=0mm. This is a very attractive feature, particularly for SRMs used in high speed applications, where iron loss could be a significant proportion of the overall loss.
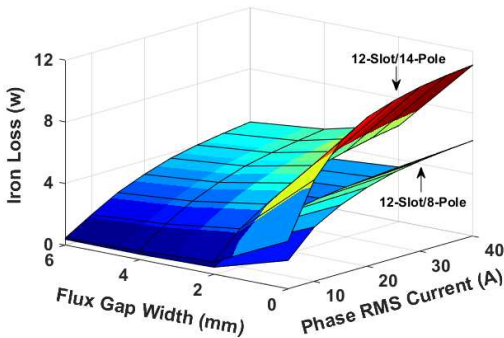

Fig. 8. Variation of iron loss against FG width and phase RMS current between the 12-slot/8-pole and 12-slot/14-pole SRMs with conventional

winding. The 3-phases are supplied with rectangular wave current with conduction angle of unipolar 120° elec., @ 400rpm.
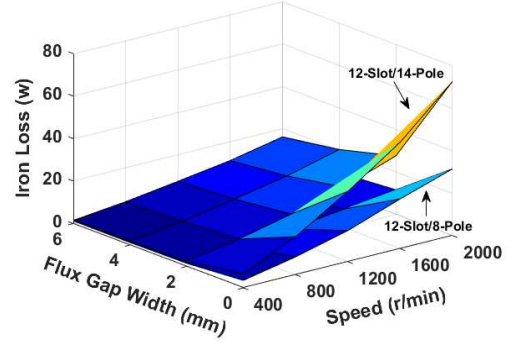

Fig. 9. Variation of iron loss against FG width and speed between the 12-slot/8-pole and 12-slot/14-pole SRM with conventional winding. 3-phases are supplied by rectangular wave current with conduction angle of unipolar 120° elec., @ $10A_{rms}$.

IV. DSRMs WITH SINEWAVE EXCITATION

A. Influence of Winding Configurations on DSRMs

1) Average Torque and Torque Ripple against Phase RMS Current

In order to use the 3-phase standard inverter, the SRMs have been supplied with sinewave currents and they are in effect doubly salient synchronous reluctance machines (DSRMs). Fig. 10 shows the average torque and torque ripple of the DSRMs with different winding configurations.
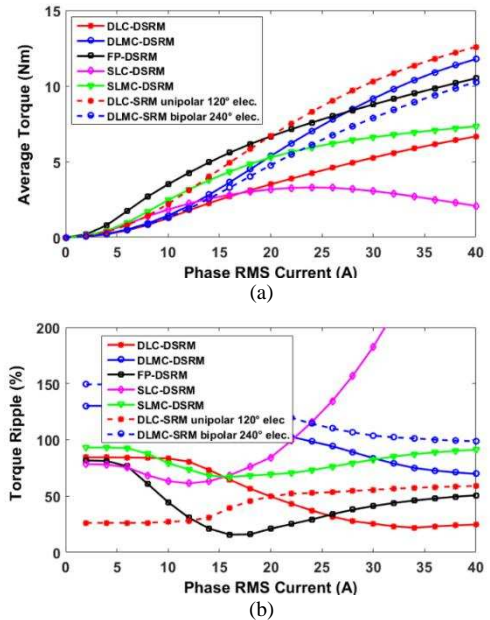

(a)

(b)

Fig. 10. Comparison of (a) average torque and (b) torque ripple coefficient against phase RMS current varying from 0A to 40A. (Solid lines stand for machines supplied by 3-phase sinewave currents. Performances of DLC-DSRM and DLMC-DSRM also compare to that supplied by rectangular wave excitation with unipolar 120°elec. conduction.).

At low current, it is found that the FP-DSRM produces higher average torque but lower torque ripple than others. In addition, the SLC-DSRM and SLMC-DSRM generate higher average torque but lower torque ripple than the DLC-DSRM and DLMC-DSRM, respectively. However, at high current, the average torque of the DLMC-DSRM becomes higher

than that of the FP-DSRM, because the FP-DSRM is more sensitive to magnetic saturation due to its SL winding structure. Similarly, both the SLC-DSRM and SLMC-DSRM produce less torque than their DL counterparts at high current levels. Therefore, it can be concluded that all the FP-DSRM, SLC-DSRM and SLMC-DSRM exhibit superior performances at low current. However, with significant longer end-winding, the FP-DSRM has much higher copper loss than both the SLC-DSRM and the SLMC-DSRM.

For completeness, the results for the DLC-SRM and DLMC-SRM supplied by rectangular wave current with their most appropriate conduction angles (from TABLE IV) have been selected as examples and compared with those obtained with sinewave excitation. It is found that the DLC winding with rectangular wave excitation can exhibit better performance, particularly at high phase current. While the sinewave excitation is more appropriate for the DLMC winding.

2) Efficiency Maps

Efficiency maps for the DSRMs with different winding configurations have been calculated from the torque speed characteristics and the losses, as shown in Fig. 11 (regions with efficiency below 50% are not shown). For this specific series of designs, a maximum peak efficiency of 76% is achieved by DLMC-DSRM between 6000 and 8000 rpm. The DLC-DSRM also achieves its maximum efficiency within the similar speed range as the DLMC-DSRM. In contrast, the SLC-DSRM and SLMC-DSRM achieve their maximum efficiencies (around 75%) over the speed range from 3000 to 4500 rpm. Furthermore, the FP-DSRM obtains a more modest efficiency of 66% at lower rotor speed around 2000rpm.
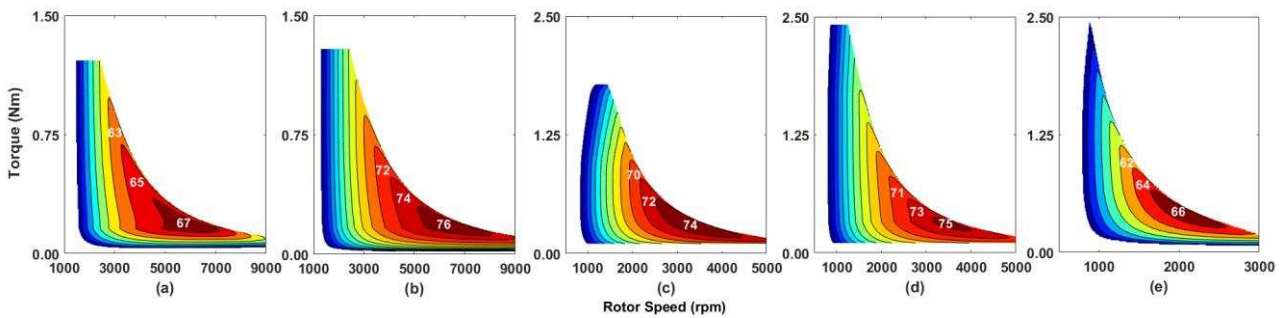

Fig. 11. Efficiency maps of SRMs when $I_{max} = 14.14A$, and $V_{DC} = 100V$. (a) DLC-DSRM, (b) DLMC-DSRM, (c) SLC-DSRM, (d) SLMC-DSRM, and (e) FP-DSRM.
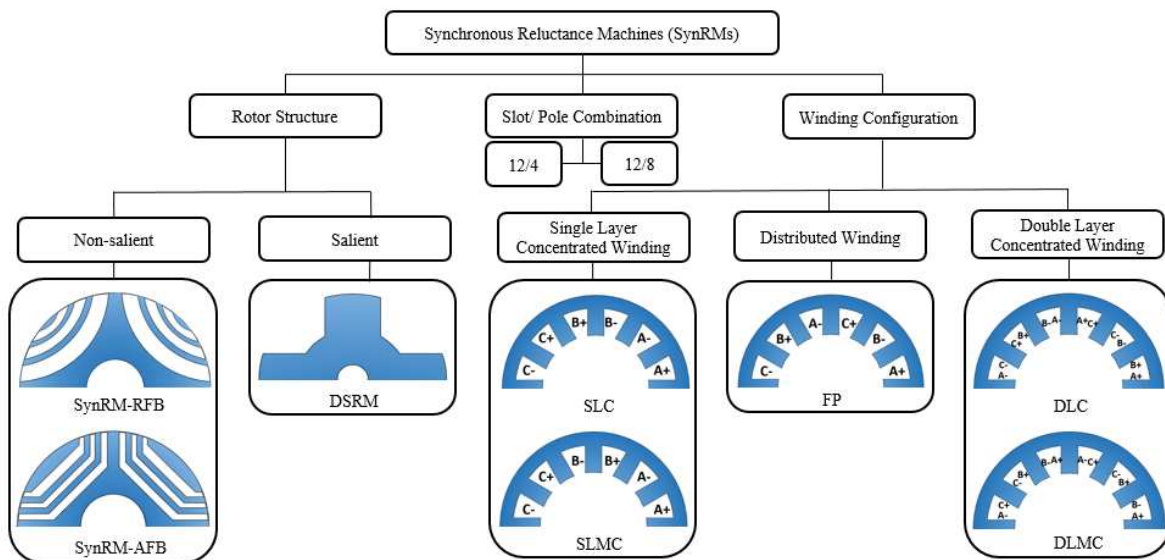

Fig. 12. Investigation variables on synchronous reluctance machines (SynRMs). SynRMs are supplied with sinewave currents.

B. Investigation of SynRMs with Different Rotor Structures

Different from the DSRMs, the most commonly investigated SynRMs employ flux barriers inside the rotors with various topologies in order to increase the saliency ratio and also the difference between d- and q-axis inductances, and hence to increase the torque capability [21] [22]. For simple industrial manufacturing, the transversally laminated rotor has been selected for investigation in this paper with both round flux barrier (RFB) and angled flux barrier (AFB). For clarity, Fig. 12 shows a diagram including rotor topologies, slot/pole number combinations and winding configurations for all the investigated SynRMs in this paper. The three SynRMs with rotor topologies: SynRM-RFBs,

SynRM-AFBs and DSRM for both the 12-slot/4-pole and 12-slot/8-pole have been investigated. In addition, the DLC/SLC windings, DLMC/ SLMC windings, as well as the FP winding have been employed.

The saliency ratio ($\zeta = \frac{L_d}{L_q}$) in TABLE V shows that the machines with the DLMC winding have the highest ζ, regardless of the rotor topologies. In addition, it has been found that ($L_\mathrm{d} - L_\mathrm{q}$) is the highest at high current levels ($40A_{rms}$). As a result, it can be predicted that the 12-slot/8-pole machines with the DLMC winding could have better machine performance than others. According to the phasor diagram of the SynRM, the power factors are obtained as well. Regardless of winding configurations, the SynRM-RFB can have the highest saliency ratio and power factors due to higher average ratio of flux barrier thickness to the combined thickness of lamination and flux barrier [22]. Moreover, the power factors of the DL winding machines are higher than those of the SL winding machines due to relatively lower synchronous inductances. This also explains why the machines with FP windings have the lowest power factors.

Accordingly, TABLE VI summarizes the appropriate rotor topologies to obtain the maximum average torque for both the 12-slot/4-pole and 12-slot/8-pole machines with different winding configurations. Moreover, the FP winding is found to be the most appropriate winding configuration for the 12-slot/4-pole machines, while the DLMC winding is the best for the 12-slot/8-pole machines. In addition, it has been found that the 12-slot/4-pole and 12-slot/8-pole machines have similar torque capability (12Nm at $40A_{rms}$) when the appropriate winding configurations and rotor topologies are employed. Furthermore, the torque performance in terms of both average torque and torque ripple of the 12-slot/4-pole 12-slot/8-pole machines with the best SynRMs and DSRMs topologies has been shown in Fig. 13. It can be found that at low current, the 12-slot/8-pole DSRMs can produce higher average torque but lower torque ripple than SynRMs. However, the average torque of both machines are similar at the high current around $40A_{rms}$, while the lower torque ripple can be achieved by the SynRMs. For 12-slot/4-pole machines, the DSRMs can have higher average torque than the SynRMs when the current is higher than $10A_{rms}$.

TABLE V COMPARISON OF SALIENCY RATIO $\frac{L_\mathrm{d}}{L_\mathrm{q}}$ AND POWER FACTORS FOR DIFFERENT 12-SLOT/8-POLE MACHINES AT $10A_{rms}$ ($I_d = I_q$)

	SynRM-RFB		SynRM-AFB		DSRM	
	$L_\mathrm{d}/L_\mathrm{q}$	Power Factor	$L_\mathrm{d}/L_\mathrm{q}$	Power Factor	$L_\mathrm{d}/L_\mathrm{q}$	Power Factor
SLC	1.787	0.676	1.639	0.638	1.635	0.621
SLMC	1.847	0.679	1.713	0.637	1.834	0.620
FP	1.523	0.576	1.135	0.508	1.680	0.567
DLC	1.459	0.778	1.122	0.741	1.787	0.745
DLMC	2.106	0.796	2.096	0.752	1.895	0.750

TABLE VI APPROPRIATE ROTOR TOPOLOGIES TO OBTAIN THE MAXIMUM AVERAGE TORQUE

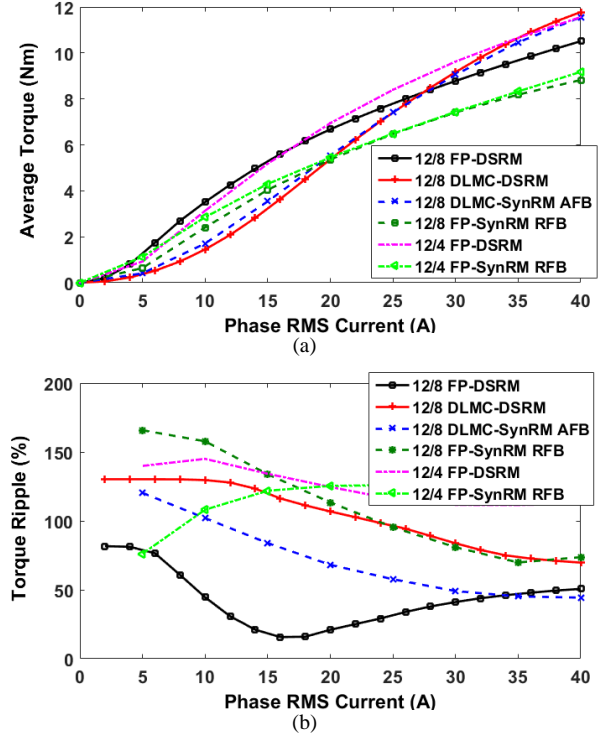|	Winding configurations				
	SLC	SLMC	FP	DLC	DLMC
12-slot/4-pole	DSRM	DSRM	DSRM	SynRM-RFB &DSRM	DSRM
12-slot/8-pole	SynRM-RFB &DSRM	DSRM	DSRM	DSRM	SynRM-AFB &DSRM

Fig. 13. Comparison between (a) average torque and (b) torque ripple of the 12-slot/4-pole and 12-slot/8-pole machines with the best SynRMs and DSRMs topologies.

V. EXPERIMENTAL VALIDATION

A. Prototypes of Reluctance Machines

In order to validate the predictions, the reluctance machine prototypes with different structures (non-modular and modular), different winding configurations (DLC/SLC and DLMC/SLMC), and different slot/pole combinations (12-slot/8-pole and 12-slot/14-pole) are constructed with the design specifications shown previously in TABLE I. Fig. 15 (a) and (b) show the wound 12-slot non-modular stators with DLC/DLMC and SLC/SLMC windings, respectively. The conventional and mutually-coupled windings can be realized with the same stator core and coils through a simple reconnection of the individual coils as detailed in Fig. 1. Fig. 14 (c) shows the wound 12-slot modular stator with SLC/SLMC windings. The common rotors of all the single and double layer variants are shown in Fig. 15 with both 8-pole and 14-pole.
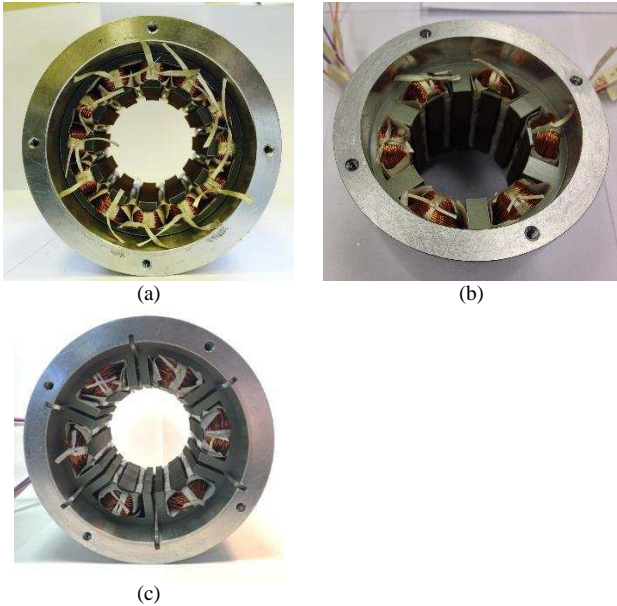
Fig. 14. 12-slot prototype reluctance machines. (a) non-modular with DLC or DLMC windings, (b) non-modular with SLC or SLMC windings, (c) modular with SLC or SLMC windings.
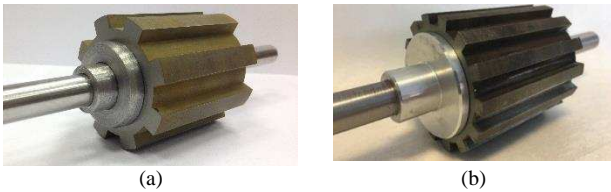

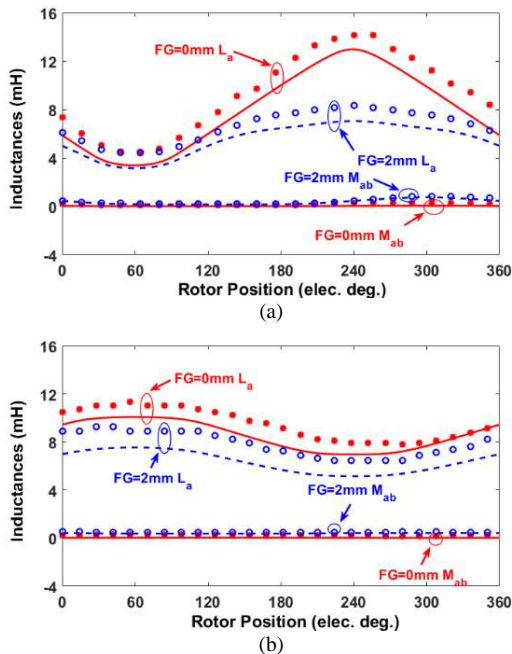Fig. 15 Salient rotors with (a) 8-pole and (b) 14-pole.

Fig. 16. Predicted and measured self- and mutual-inductances against rotor position at 1A AC current. (a) 12-slot/8-pole SRM with FG=0mm and 2mm. (b) 12-slot/14-pole SRM with FG=0mm and 2mm (lines: predicted results, and marks: measured results).

B. Measurement of Self- and Mutual-Inductances

The self- and mutual-inductances of the reluctance machines are measured according to the method in [18] at 1A AC current. The measured phase resistances of the SL- and DL-SRMs are 1.48Ω and 1.32 Ω, respectively. Fig. 16 shows the results for non-modular and modular CSRM with both 8

and 14-poles, while Fig. 17 shows the results for the 12-slot/8-pole DSRMs with different winding configurations. The measured results are generally slightly higher than the predicted ones mainly due to the fact that the end-windings have not been taken into account in the predictions.
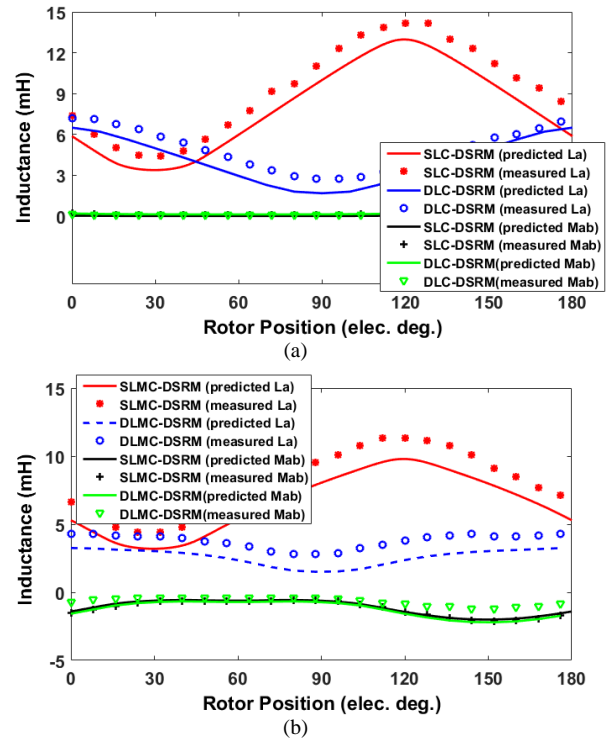

Fig. 17. Measurement of self- and mutual-inductances of the 12/8 DSRMs with different windings at 1A dc current. (a) Conventional winding DSRMs, (b) Mutually-coupled winding DSRMs.

C. Measurement of Static Torque

The method in [23] has been adopted for undertaking the static torque measurement in this paper. According to the current waveforms with different conduction angles as shown in Fig. 4, the on-load torques can be measured at different rotor positions. By way of example, the results for SLC-SRM and SLMC-SRM are shown in Fig. 18. The aligned rotor position of phase A can be tested when the phase A is excited. The phase RMS current of all the rectangular wave excitations is 4A, and the dc current is injected into each phase at different rotor positions corresponding to the current waveforms.
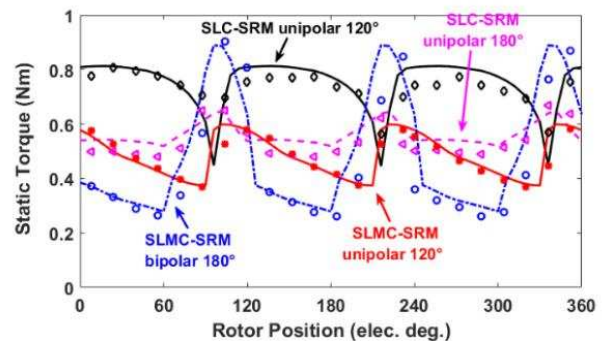

Fig. 18. Predicted and measured static torques versus rotor position at 4A phase RMS current. (Lines: predicted results, marks: measured results).
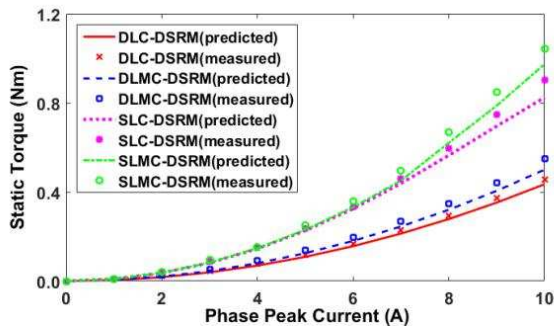
Fig. 19. Predicted and measured static torque as a function of phase peak current.

In order to measure the static torque of the DSRM, three phases are supplied with dc currents such as $I_A = I$, $I_B = I_C = -1/2I$, where I is variable and controllable by the power supply. Fig. 19 shows a comparison between predicted and measured static torques for both the DL- and SL-DSRMs, at phase peak currents between 1A and 10A. In the torque measurements, the rotor is fixed at an angular position which corresponds to the maximum average torque (45 elec. deg. if magnetic saturation does not occur). It can be found that the measured results are in good agreement with the predicted results.

VI. CONCLUSION

In this paper, the recent developments in the reluctance machines have been summarized. The investigated machines have different winding configurations (SLC, SLMC, DLC, DLMC and FP), different excitation methods (rectangular wave and sinewave) and also different rotor structures.

The rectangular wave excitation with conduction angle of unipolar 120° elec., unipolar 180° elec., bipolar 180°elec., bipolar 240°elec. and bipolar 360° elec. have been adopted for all the non-modular SRMs with different winding configurations. In addition, the most appropriate conduction angle has been obtained for all the 12-slot/8-pole machines at different current levels. Comparing to non-modular 12-slot/8-pole SRMs, it has been found that the modular 12-slot/14-pole SRMs with both the SLC and SLMC winding configurations can achieve similar average torque for the same copper loss (phase current) but with lower torque ripple and also lower iron loss.

With sinewave excitation, the results demonstrated that at low phase current, the FP-DSRM has the best torque performance. In addition, the SLC-DSRM and SLMC-DSRM produce higher average torque with lower torque ripple than their DL counterparts, respectively. However, due to the onset magnetic saturation, the performance of the FP-DSRM, SLC-DSRM and SLMC-DSRM deteriorates markedly with increasing phase RMS current, making them less attractive at high phase current. While with less sensitivity to magnetic saturation, the DLMC-DSRM performs well at high current levels, producing higher average torque than other machines. From a dynamic perspective, within the contest of this particular design study, the DLMC-DSRM yields the highest peak efficiency. Furthermore, both the 12-slot/8-pole and 12-slot/4-pole

DSRM have been compared to the SynRMs with both AFB and RFB. Accordingly, most appropriate rotor structures have been obtained for the machines with different slot/pole combinations and winding configurations.

References

[1] T. J. E. Miller, "Optimal design of switched reluctance motors," IEEE Trans. Ind. Electron., vol. 49, no. 1, pp. 15-27, Feb. 2002.

[2] G. J. Li, J. Ojeda, E. Hoang, M. Lecrivain and M. Gabsi, "Comparative studies between classical and mutually coupled switched reluctance motors using thermal-electromagnetic analysis for driving cycles," IEEE Trans. Magn., vol. 47, no. 4, pp. 839-847, Apr. 2011.

[3] D. A. Torrey, X.-M. Niu and E. J. Unkauf, "Analytical modelling of variable-reluctance machine magnetisation characteristics," Proc. IEE—Elec. Power Appl., vol. 142, no. 1, pp. 14-22, Jan. 1995.

[4] A. L. M. d. Santos, J. Anthonis, F. Naclerio, J. J. C. Gyselinck, H. V. d. Auweraer and L. C. S. Goes, "Multiphysics NVH modeling: simulation of a switched reluctance motor for an electric vehicle," IEEE Trans. Ind. Electron., vol. 61, no. 1, pp. 469-476, Jan. 2014.

[5] S. A. Long, Z. Q. Zhu and D. Howe, "Effectiveness of active noise and vibration cancellation for switched reluctance machines operating under alternative control strategies," IEEE Trans. Energy Convers., vol. 20, no. 4, pp. 792-801, Dec. 2005.

[6] D. A. Staton, W. L. Soong and T. J. E. Miler, "Unified theory of torque production in switched reluctance and synchronous reluctance motors," IEEE Trans. Ind. Appl., vol. 31, no. 2, pp. 329-337, Mar./Apr. 1995.

[7] D. E. Cameron, J. H. Lang and S. D. Umans, "The origin and reduction of acoustic noise in doubly salient variable-reluctance motors," IEEE Trans. Ind. Appl., vol. 28, pp. 1250-1255, Nov./Dec. 1992.

[8] C. Wei, P. Pillay, Z. J. Tang and A. M. Omekanda , "Low-vibration design of switched reluctance motors for automotive applications using modal analysis," IEEE Trans. Ind. Appl., vol. 39, no. 4, pp. 971-977, Jul./ Aug. 2003.

[9] R. R. Moghaddam, F. Magnussen and C. Sadarangani, "Theoretical and experimental reevaluation of synchronous reluctance machine," IEEE Trans. Ind. Electron., vol. 57, no. 1, pp. 6-13, Jan. 2010.

[10] X. Ojeda, X. Mininger, M. Gabsi and M. Lecrivain, "Sinusoidal feeding for switched reluctance machine: application to vibration," in Proc. ICEM, Vilamoura, Portugal, Sept. 2008.

[11] G. Pellegrino, F. Cupertino and C. Gerada, "Barriers shapes and minimum set of rotor parameters in the automated design of Synchronous Reluctance machines," in Int. Conf. Electric Machines & Drives, pp. 1204-1210, May 2013.

[12] A. Vagati, M. Pastorelli, G. Francheschini and S. C. Petrache, "Design of low-torque-ripple synchronous reluctance motors," IEEE Trans. Ind. Appl., vol. 34, no. 4, pp. 758-765, Jul./Aug. 1998.

[13] X. B. Liang., G. J. Li, J. Ojeda, M. Gabsi and Z. X. Ren, "Comparative study of classical and mutually coupled switched reluctance motors using multiphysics finite-element modeling," IEEE Trans. Ind. Electron., vol. 61, no. 9, pp. 5066-5074, Oct. 7, 2013.

[14] R. R. Moghaddam and F. Gyllensten, "Novel high-performance SynRM designmethod: an easy approach for a complicated rotor topology," IEEE Trans. Ind. Electron., vol. 61, no. 9, pp. 5058-5065, Sept. 2014.

[15] P. B. Reddy, A. M. El-Refaie, K. K. Huh, J. K. Tangudu and T. M. Jahns, "Comparison of interior and surface PM machines equipped with fractional-slot concentrated windings for hybrid traction applications," IEEE Trans. Energy Convers., vol. 27, no. 3, pp. 593-602, May 2012.

[16] A. M. El-Refaie, T. M. Jahns and D. W. Novotny, "Analysis of surface permanent magnet machines with fractional-slot concentrated windings," IEEE Trans. Energy Convers., vol. 21, no. 1, pp. 34-43, Feb. 2006.

[17] A. M. El-Refaie, "Fractional-slot concentrated-windings synchronous permanent magnet machines: opportunities and challenges," IEEE Trans. Ind. Electron., vol. 57, no. 1, pp. 107-121, Sept. 2010.

[18] G. J. Li, X. Y. Ma, G. W. Jewell and Z. Q. Zhu, "Influence of conduction angles on single layer switched reluctance machines," IEEE Trans. Magn., vol. 52, no. 12, pp. 1-11, Jul. 2016.

[19] X. Y. Ma, G. J. Li, G. Jewell and Z. Q. Zhu, "Comparative study of short-pitched and fully-pitched SRMs supplied by sine wave currents," in ICIT15, Sevilla, Spain, Mar. 17-19, 2015.

[20] X. Y. Ma, G. J. Li, G. W. Jewell, Z. Q. Zhu and H. L. Zhan, "Performance comparison of doubly salient reluctance machine topologies supplied by sinewave currents," IEEE Trans. Ind. Electron., vol. 63, no. 7, pp. 4086-4096, Mar. 2016.

[21] T. A. Lipo, "Synchronous reluctance machines- a viable alternative for AC drives," Wisconsin electric machines and power electronics consortium, Madison, USA, May 1991.

[22] D. A. Staton, T. J. E. Miller and S. E. Wood, "Maximising the saliency ratio of the synchronous reluctance motor," Elec. Power Appl, IEE Proc. B, vol. 140, no. 4, pp. 249-259, Jul. 1993.

[23] Z. Q. Zhu, "A simple method for measuring cogging torque in permanent magnet machines," in IEEE Power & Energy Society General Meeting,, Jul. 26-30, 2009, pp. 1-4.

[24] X. Liu, Z. Q. Zhu, M. Hasegawa, A. Pride and R. Deodhar, "Investigation of PWMs on vibration and noise in SRM with sinusoidal bipolar excitation," in 21st IEEE-ISIE, Hangzhou, China, 28- 31 May, 2012.

G. J. Li (M'10) received his BEng, MSc and PhD degrees in electrical and electronic engineering from the Wuhan University, China, in 2007, University of Paris XI, France, in 2008, and the Ecole Normale Supérieure (ENS) de Cachan, Paris, France, in 2011, respectively. He joined the University of Sheffield in June 2012 as a post-doctoral research associate at EMD Group. Since September 2013, he took up a Lectureship in Electrical Engineering within the EMD Group at the University of Sheffield and became a Senior Lecturer in Nov. 2017. His main research interests include the design, fault analysis and thermal management of electrical machines for renewable energy, automotive, more electrical aircraft, etc.

G. W. Jewell received the B.Eng. and Ph.D. degrees in Electrical Engineering from The University of Sheffield, Sheffield, U.K., in 1988 and 1992, respectively. Since 1994, he has been a member of Academic Staff in the Department of Electronic and Electrical Engineering, The University of Sheffield, where he is currently a Professor of Electrical Engineering, Head of Department and Director of the Rolls-Royce University Technology Centre in Advanced Electrical Machines. His research interests include the modelling and design of a wide variety of electromagnetic devices, notably electrical machines for aerospace and high-temperature applications. Professor Jewell held an Engineering and Physical Sciences Research Council Advanced Research Fellowship from 2000 to 2005 and a Royal Society Industry Fellowship with Rolls-Royce from 2006 to 2008.

X. Y. Ma received the B.Eng. degree in electrical engineering from The University of Sheffield, Sheffield, U.K., in 2012, and the M.Sc. degree in sustainable energy systems from The University of Edinburgh, Edinburgh, U.K., in 2013. She is currently working toward Ph.D. degree in the Department of Electronic and Electrical Engineering, The University of Sheffield, Sheffield, U.K. Her current research interest is switched reluctance machines and synchronous reluctance machines.

Z.Q. Zhu received the B.Eng. and M.Sc. degrees in electrical and electronic engineering from Zhejiang University, Hangzhou, China, in 1982 and 1984, respectively, and the Ph.D. degree in electrical and electronic engineering from The University of Sheffield, Sheffield, U.K., in 1991. Since 1988, he has been with The University of Sheffield, where he is currently a Professor with the Department of Electronic and Electrical Engineering, Head of the Electrical Machines and Drives Research Group, Royal Academy of Engineering/Siemens Research Chair, Academic Director of Sheffield Siemens Wind Power Research Centre, Director of Midea Electrical Machines and Controls Research centres, Director of Sheffield CRRC Electric Drives Technology Research Centre. His current major research interests include the design and control of permanent-magnet brushless machines and drives for applications ranging from automotive to renewable energy. He is Fellow of Royal Academy of Engineering, Fellow of IEEE, and Fellow of IET.